Chapter 4

Complex Langevin dynamics of spherical dimers

Much of the calibration theory discussed in Chapter 2 assumes that the target particle in question is a single sphere, one who's scattering and motion is easily computed. However, while working with dense colloidal suspensions, one often ends up trapping more than one sphere. Li and Arlt [9] studied the case of two microspheres trapped in a single OT and found that multiple trapped beads could be mistaken for a single trapped bead with altered trap stiffness. Theoretical studies on the case of two trapped microspheres by Xu *et al.* [21] employed a ray-optics based model to show that the two trapped beads are brought into physical contact with each other by optical forces and they also calculated the axial equilibrium positions of the two trapped beads as a function of their size. Experiments in [11] confirmed that the two trapped beads indeed experience different trap stiffnesses in the vicinity of the same potential well. There are further discussions looking into the dynamics of a whole host of asymmetrically shaped particles [5, 10, 17], their results all showing that predicting the behaviour an arbitrary shaped particle comes with great difficulty due to the fact that the optical force is dependent on a greater number of variables such as orientation and size factors.

With the initial goal of the PhD being to induce nucleation events via a spherical micro-rotor the goal of this chapter was to - in a limited capacity simulate and investi-

gate the influence of a second particle being bound to our target sphere. The choice of a dimer, instead of an amorphous solid that might better represent a growing crystalline solid, allows us to consider how the dynamics of the aggregate change by varying the size factor. We build upon the works of Vigilante *et al* [19] to consider asymmetric dimers and how varying size parameters alters the dynamics and additionally makes characterising their interactions within an optical trap more cumbersome. Attempting to simulate an amorphous aggregate is rather difficult as calculating the optical force and torque is computationally slow and orientation specific.

4.1 Positional and Orientational dependence of Trapping forces

If we wanted to start from first principles and determine the trap strength on our target particle the first step would be to locate the equilibrium position relative to the trap focus. For a single sphere it is easy to enough to understand that its centre of mass will be drawn to focal point of the laser due to gradient forces, once there the force is analogous to a harmonic spring with a fixed trap stiffness. Now, if we consider instead a dimer, we now have two spheres both being drawn to the focus along by the same gradient force; in addition the scattering force is significantly more complex due to both spheres scattering the electromagnetic fields. This mutual scattering between individual spheres is what makes simulating spherical aggregates far more difficult compared to a single sphere, and even harder still to predict the position where the dimer's centre of mass is in equilibrium.

Because the scattering force is only significant in the direction of beam propagation the potential well in the transverse plane can still be assumed to be harmonic around the central beam axis. The axial optical force cannot be assumed to behave as a simple harmonic trap. The methodology for computing optical forces has been covered extensively for a number of different trapping conditions [12], so it is relatively easy to compute the trapping force and determine where a simple sphere would be located relative to focal point of the laser by finding the position that minimises the net optical

force in a negative feed back loop ($\delta F/\delta x < 0$) - we can assume that for a dielectric sphere the optical torque is negligible. For a dimer (or any arbitrary spherical aggregate), we now must consider both its position and orientation and find where the net optical force and torque are minimised.

Simulation Parameters As a paradigmatic example, consider a dimer suspended in water ($n_p = 1.59, n_m = 1.33$) located at the focus of a Gaussian beam (more specifically a Laguerre-Gaussian beam of mode $[0, 0]$), the beam is focused by a objective with numerical aperture of 1.2 and is x polarised. The size ratio of the two sphere's is given by $a_I/a_{II} = 2$ where a_I is kept at 1 μm unless specified otherwise; the dimer's orientation is given by a unit vector connecting the centres of both spheres, we define the 'standard' orientation as being aligned with the direction of beam propagation direction - and therefore the 'inverted' orientation is defined when the dimer is orientated against the direction of beam orientation (see figures 4.1(b) and (d)).

After computing its T-matrix via *mstm* and supplying that to *ott* we compute the optical force exerted by a 50 mW laser via (**??**) in the axial direction while the dimer is in its 'standard' orientation. As expected we see a single point where the dimer will be in equilibrium, the linear fit in fig. 4.1 (a) indicates a that the force can be modelled as a harmonic potential close to the equilibrium position ($F_z \approx -\kappa_z z$). The second point where the axial force goes to 0 cannot be considered as equilibrium position as the positive gradient indicates that the trap is unstable unless Brownian motion is ignored.

We repeated the same calculation but now while the dimer is in its 'inverted' orientation, instead of a single point where the optical force is minimised we see that there are instead two separate equilibrium positions, one above the focus and one below the focus. In this particular example the two positions are far enough apart that both can be considered as separate harmonic traps.

We can see that both equilibrium positions have comparable axial trap stiffness (κ_z), however the difference in the transverse trap stiffness (κ_x) is far more noticeable. The same dimer was trapped at each of the axial equilibrium positions and the transverse force was evaluated. While in all three cases the dimer can be trapped the linear range

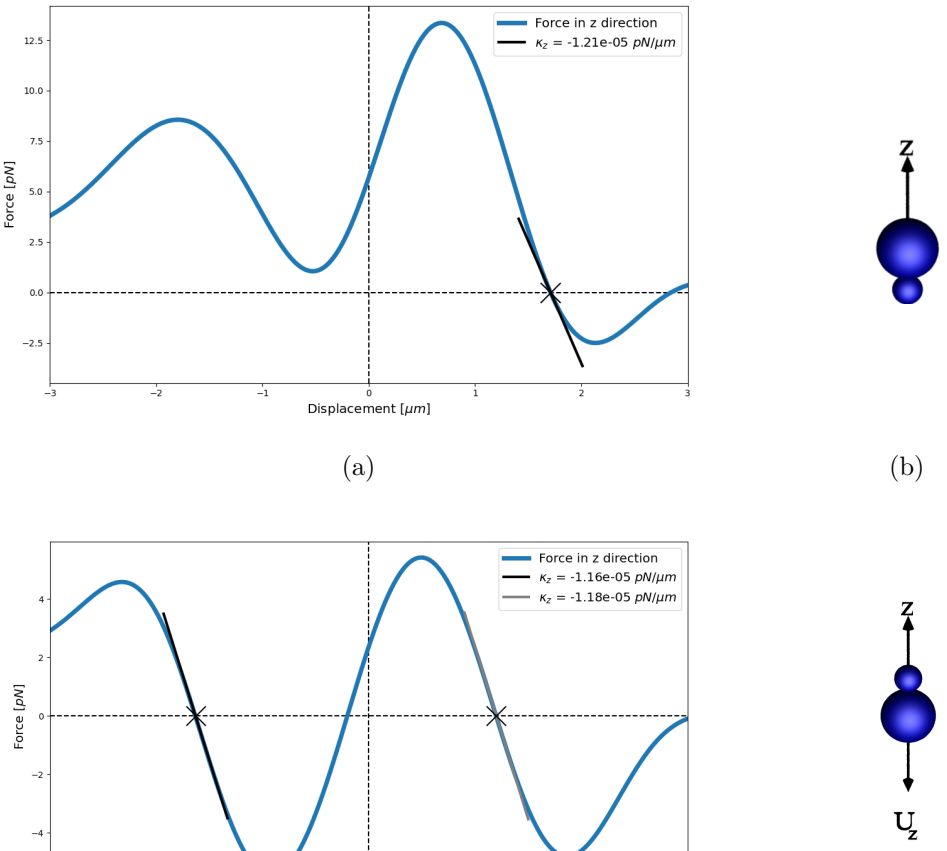

Figure 4.1: Plots of force vs displacement of the centre of mass of the dimer (µm) for the case of a dimer of size ratio 2. (a) is the case where the dimer is in its' 'standard' orientation, where the dimer is trapped at $z = 1.71\ \mu m$. (c) is the case where the dimer is in its' 'inverted' orientation, the dimer is trapped at two positions: $z = 1.20\ \mu m$ & $z = -1.63\ \mu m$. (b) and (d) are renders to visualise the dimer orientation are shown below each plot. The black lines on each force-curve is a linear fit with the slope being reported as the trap stiffness in the legend.

where that would typically associated with a stable trap is far narrower in the 'standard' orientation compared to the 'inverted' cases. This highlights one of the challenges involved with studying asymmetric particles, even though its a simple enough process to trap them they maybe characterised very differently depending on their relative

position and orientation towards the focus. This can have a significant impact on rheological studies - or attempting to probe any local property - as the variance in trap strength can result in large errors over repeated measurements.

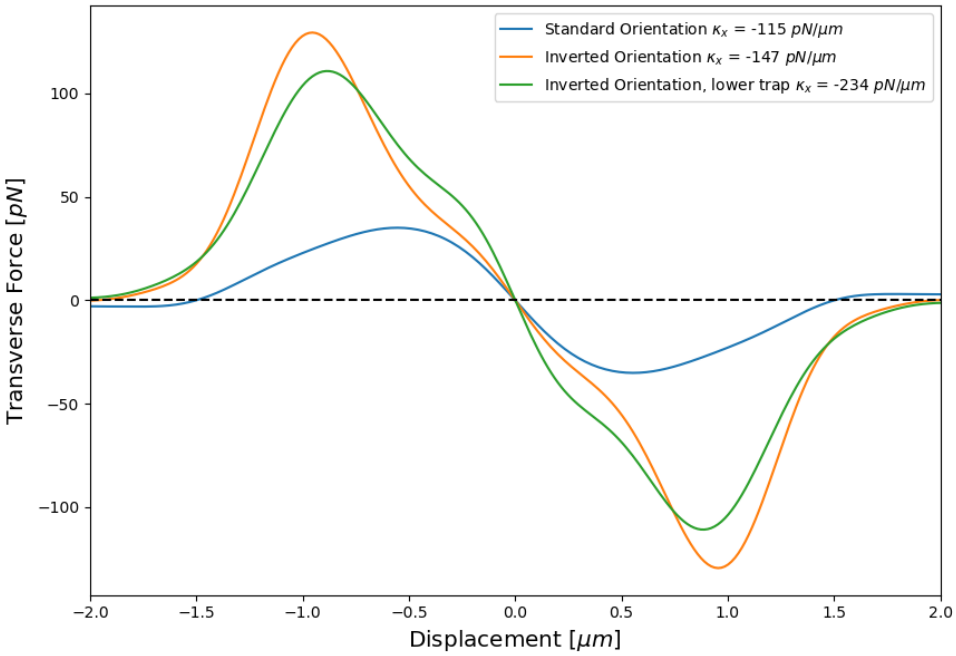

Figure 4.2: Plots of force vs displacement of the dimer's centre of mass spheres, where a positive force indicates the dimer is directed right on the x-axis, and vice versa for a negative force. The same simulation parameters are used here as in fig 4.1(a) and (c). The blue curve representing the force response for a dimer in its standard orientation, orange being the inverted case, and green the same case but placed below the focus.

For completeness the harmonic traps were located for dimers across a range of size ratios - from $a_I/a_{II} = 1$ to $a_I/a_{II} = 10$ - while also recording the trap stiffness for each trap. The same simulation parameters are used here as for figures 4.1 & 4.2. As shown in Fig. 4.3 a_{II} decrease the dimer begins to approximate a single homogenous sphere - at least in terms of location and trap strength. However, for intermediate sized dimers (between $a_I/a_{II} = 1.1$ to $a_I/a_{II} = 4$), a second equilibrium position is found below the trapping focus. Previous work using the ray-optics model have confirmed even in the case that two spheres begin separated the electric field will align the particles as such that they make contact and are trapped together about a single trapping position [21]. Furthermore it has been shown through proper manipulation of the Gaussian or Bessel beam modes that any number of trapping potentials can be developed [16] for nanoparticles. This result however, is the first example of an orientation dependent trapping situation using only a TEM_00 beam. Typical experimental arrangements cannot determine much information on the axial position of a trapped particle relative to the trap focus; this result indicates not only that dimers can be trapped in multiple axial positions but also their trapping behaviour is heavily dependent on said axial position. As such it is necessary that positional information in the z-axis can be elucidated if multiple spheres are trapped simultaneously.

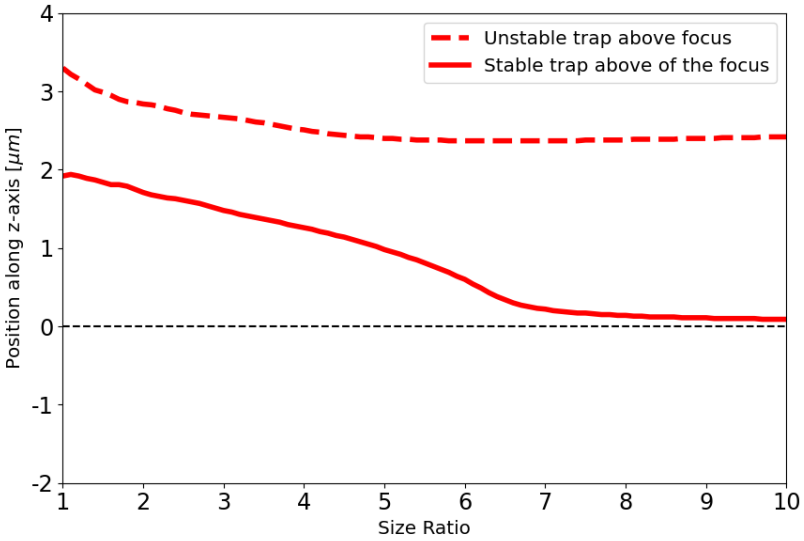

(a)

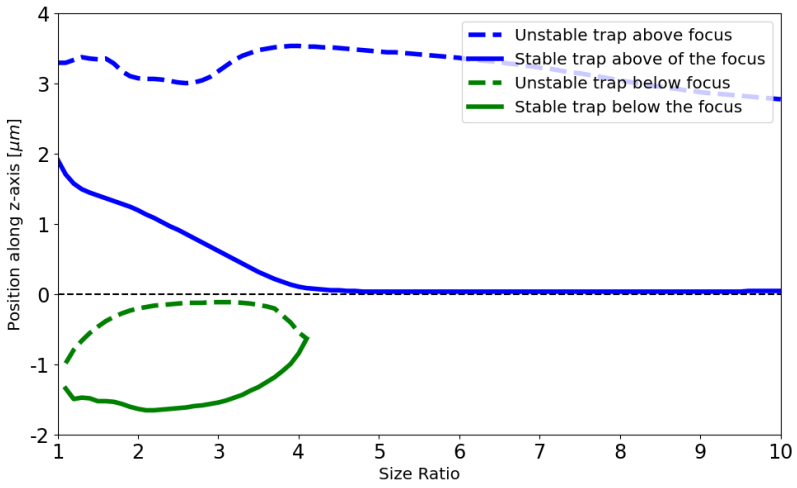

(b)

Figure 4.3: Equilibrium positions of optically trapped dimers with varying size ratio, dashed lines represent unstable traps whereas solid lines are for stable equilibrium positions. (a) shows that dimers while in their 'standard' orientation will always have a single equilibrium position. (b) shows that when the same dimer is in its' 'inverted' orientation can be trapped in two axial positions, one below the focus and one above the focus.

4.1.1 Non-trivial equilibrium configurations

Computing the equilibrium positions when a dimer is aligned with the electric field is relatively simple as the orientational torque is minimised (see Eq.**??**), meaning once trapped the dimer is unlikely to change orientation enough to escape the trap. However, that does not rule out the possibility that there is a stable configuration where the orientation not strictly vertical, in fact most experimental work with symmetric nano-dimers will trap them lying perpendicular to the beam direction [1, 14]. Unlike in Sec. 4.1 we cannot simply measure the optical force and torque as the parameter space is too large and determining if a particular position and orientation is stable is not clear based solely on force and torque measurements [4]. Using the same simulation parameters as before we ran a number short simulations (total simulation time was 0.005 s) with the laser power increased to 500 mW. Each simulation started with the dimer in a different starting position and orientation, due to the high laser power the dimers either escaped the trap or were stably trapped. The $z - \theta$ phase space - where θ is the angle between the direction of beam propagation and the dimer's orientation vector ($\theta = 0°$ is the 'standard' orientation) - can be divided into different regions depending on which equilibrium configuration is reached.

Interestingly while the trap strength of these off-axis traps are similar in magnitude to the vertically aligned dimers, but when the laser power is lowered (around 5 mW) the traps become metastable; after reaching its' equilibrium configuration the particle behaves similarly to a typically trapped dimer but the trapping potential is small enough that the dimer escapes in as little time as less than a second or after nearly a full 3 seconds. Running similar simulations but for vertical configurations sees the dimer remaining trapped, even after 30 seconds of run time, indicating that the trapping potential is far greater than the thermal energy. This suggests that the reason this off-axis configuration is due to the rotational motion more than translational motion. If the overall potential depth could be characterised then dimers placed into this orientation could be used as a micro-scale temperature alarm, where by fine tuning of the dimer's parameters would allow you to construct a potential well that can only be escaped when the local fluid temperature exceeds a certain maximum value.

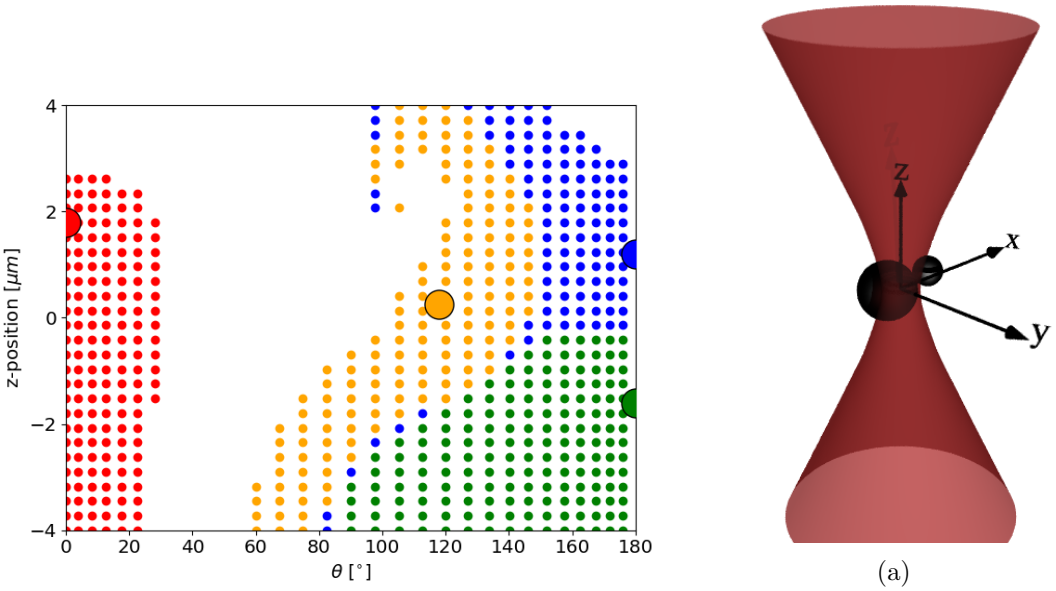

(a)

Figure 4.4: Map of $z - \theta$ phase space using a dimer of size ratio 2 with a laser power of 500 mW ($\theta = 0\circ$ is the 'standard' orientation and $\theta = 180°$ is the 'inverted' orientation). The stable configurations are indicated by the larger circles and the starting conditions are colour coded to match the stable point they end up in. Right hand render shows a dimer in its off-axis configuration.

4.2 Continuous rotational motion due to second-order scattering

One aspect that has yet to be covered in depth with regards to spherical aggregates of any construction is their interaction with circularly polarised light. For homogenous spheres the optical torque is regarded as being negligible as the spin density cannot impart angular momentum while propagating in a homogenous medium. Dimers however, have been shown to experience an optical torque [1, 14, 19] while trapped in a circular polarised beam.

First we wanted to confirm that the rotation seen in our simulations is based on the polarisation of the trapping beam. To that end, we simulated the motion of an optically trapped dimer in beams of varying polarisation ($NA = 1.2$, $P = 100\ mW$), the dimer is composed of polystyrene ($n_p = 1.59$, $n_m = 1.33$). Each simulation was run for 1 second ($\Delta t = 10^{-}5$) and at the end we looked at the orientational time series; the dimer's orientation is recorded as a quaternion which can be easily converted to a

3-dimensional rotation matrix. By considering only the transverse components ($U_{1,x}$, $U_{1,y}$, $U_{2,x}$, & $U_{2,y}$) of the rotation matrix and taking the Fourier transformation of their time series reveals the rotational frequency. The laser power is set to 100 mW to avoid large thermal fluctuations and so that the Fourier series of the transverse components approximates $\delta(\omega_{rot} - f)$ - the Dirac delta function centred at the rotational frequency ω_{rot}.

$$\begin{aligned} q(t) \rightarrow R(t) &= \begin{pmatrix} U_{1,x}(t) & U_{2,x}(t) & U_{3,x}(t) \\ U_{1,y}(t) & U_{2,y}(t) & U_{3,y}(t) \\ U_{1,z}(t) & U_{2,z}(t) & U_{3,z}(t) \end{pmatrix} \\ &\rightarrow \int_{-\infty}^{\infty} R(t) e^{-i2\pi f t} dt = \begin{pmatrix} \delta(\omega_{rot} - f) & \delta(\omega_{rot} - f) & \delta(f) \\ \delta(\omega_{rot} - f) & \delta(\omega_{rot} - f) & \delta(f) \\ \delta(f) & \delta(f) & \delta(f) \end{pmatrix} \end{aligned} \tag{4.1}$$

If the rotational frequency was not immediately obvious the simulation was repeated but over a longer simulation time. Four different size ratio of dimers were studied, both in their 'standard' and 'inverted' orientations. The results of this are displayed in Fig. 4.5:

This shows us that these optical rotations are polarisation dependent and not merely an example of the dimer scattering light asymmetrically. The question then becomes, by what mechanism is the angular momentum of the trapping beam being transferred to the dimer.

The rotation was first noted by Vigilante and co-workers who only considered this behaviour for a symmetric dimer [19]. In their work they attribute this to spin-curl effects, in which the curl of the spin density leads to a second order optical force that orbits around the beams central axis [22]. While several papers have demonstrated this phenomena [20, 23, 24] it was only properly formalised by by [15]. In which they showed that the seemingly random trajectory of a trapped sphere was biased by the polarisation state of the trapping beam. While not immediately evident from the trajectory the helicity of the trapping beam was revealed by computing the particle's

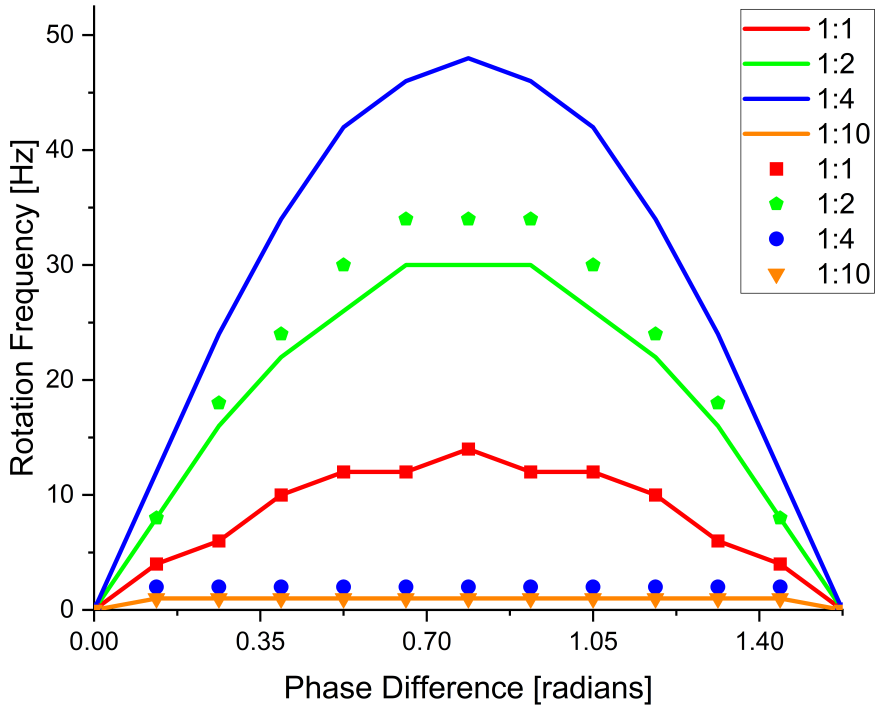

Figure 4.5: Rotation frequency vs component phase difference for differently sized dimers. The solid lines represent the rotation rate experienced while the dimer is in its standard orientation, whereas the solid points are for the case where the orientation is inverted. Laser power = 100 mW.

probability flux using.

$$j(r) = \frac{1}{N-1} \sum_{j=1}^{N-1} \frac{r_{j+1} - r_j}{\tau} \delta_{sigma_j} \left(r - \frac{r_{j+1} + r_j}{2} \right) \tag{4.2}$$

where δ_{σ_j} is the kernel of an adaptive density estimator [18]. (4.2) describes the direction a trapped sphere is most likely move in given our statistical knowledge of the trajectories probability density function. A finite estimation of the density function $p(r)$ is used in [15].

$$p(r) = \frac{1}{N} \sum_{j=1}^{N} \delta_{\sigma_j}(r - r_j) \tag{4.3}$$

The probability flux reveals a biased motion in the trajectory of a single sphere (see Fig. 4.6). This biased motion results in a slight orbital motion about the central axis of the trapping beam, the orbital frequency is shown to be proportional to the polarisation state of the trapping beam.

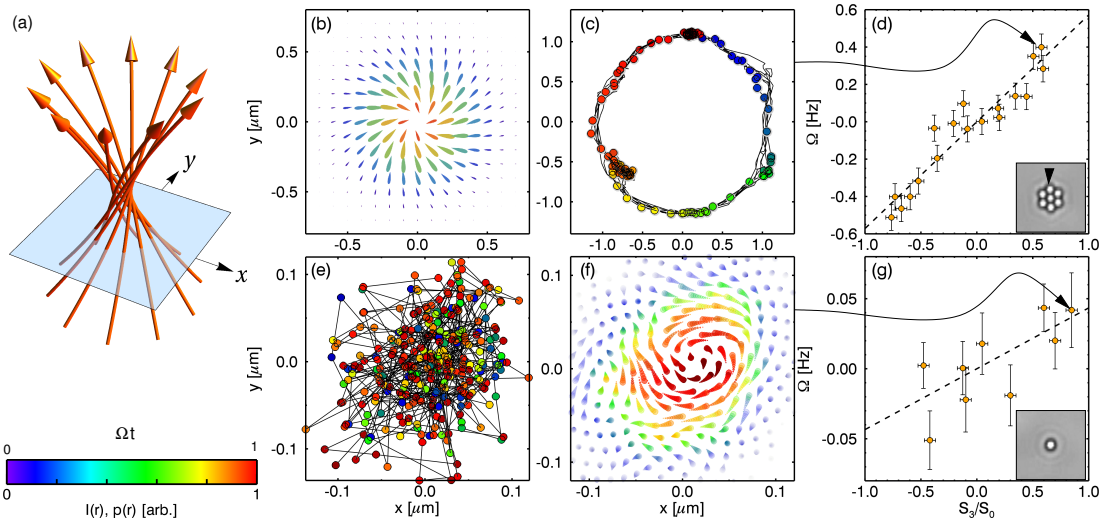

Figure 4.6: Figure reused from [15]. (a) shows how the momentum density of a Gaussian beam is twisted while using circularly polarised light. The top row (figures (b)-(d)) shows a 7 sphere cluster trapped in a circularly polarised beam. Due to the clusters asymmetric susceptibility to polarization the cluster rotates in the $x-y$ plane. Whereas the bottom row (figures (e) - (g)) show the similar results for a single sphere. In this instance the sphere does not rotate but instead orbits the beam axis. In both instances the motion is proportional to the degree of polarisation (see figures (d) and (g)) but for the single sphere this motion is only revealed when using (4.2) & (4.3). Reused with permission from author

While the results from [15] suggest that the optical rotation seen in asymmetric dimers is attributed to the same spin-curl forces there are several discrepancies that cannot be explained purely by the spin-curl force. Firstly, there is the question of how the spin-curl force results in an optical torque: Comparing figures 4.6(c) and (e) we can see that the behaviour of the 7 sphere cluster rotates about the central axis whereas the single sphere has an only slight orbital bias in its motion. The authors attributed this to the fact that the cluster is scattering light where the spin-curl force is more substantial due to it having a wider profile. This would suggest that particles' whose longer axis lies in the plane perpendicular to the direction of propagation should

experience any notable degree of torque. And indeed this appears to be the case for a number of experiments involving nano-dimers and ellipsoidal particles [1, 14].

It does raise the question of how come our simulations show that despite the dimer being orientated so their long axis' align with the parallel to the direction of propagation they still readily rotate. You would not expect that the addition of a single additional sphere should drastically adjust the torque especially if said sphere is relatively small. However when we measured the optical torque of a single sphere and a dimer - $a_I/a_{II} = 10$ - we found the exact opposite. In both cases we used the same trapping beam as used for figure 4.5 but with a circularly polarised beam. Both the sphere and dimer were rotated in the $x-z$ plane and the all three components of the optical torque were recorded.

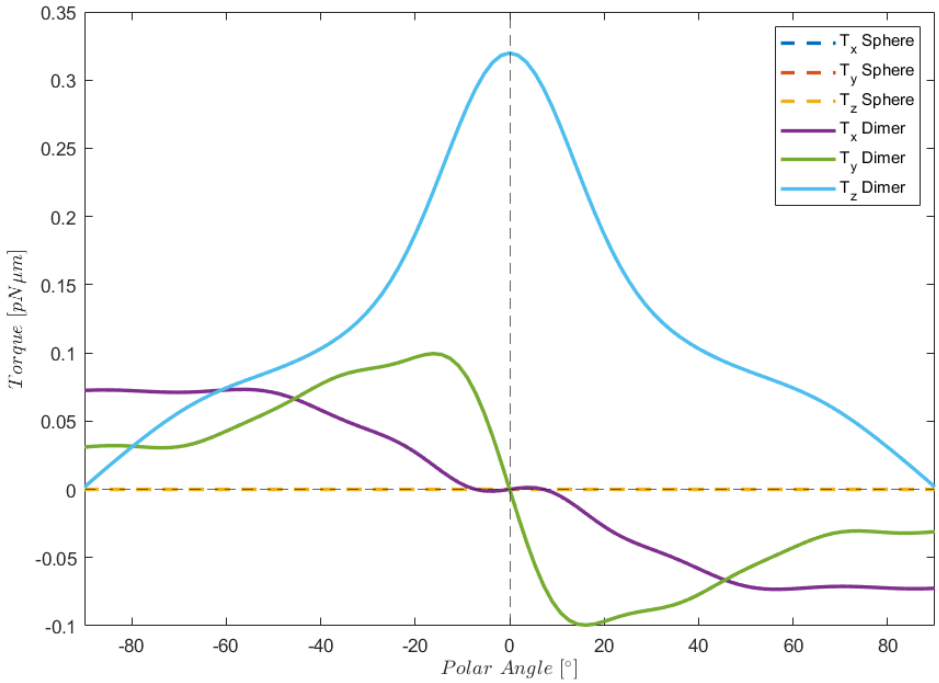

Figure 4.7: Optical toque experienced by a dimer ($a_I/a_{II} = 10$) and a single isotropic sphere. Both were rotated in the $x-z$ plane and the angle between U_z and the beam axis gives the polar angle.The solid lines denote the torque experienced by the dimer whereas the dashed lines represent the torque experienced by the sphere.

It should be noted that the difference in magnitude is not clearly shown in figure 4.7.

In truth, the optical torque acting on the dimer 10^{13} times greater than the torque applied to the single sphere. The torques about the x and y axis can be somewhat understood as the second sphere is being drawn back towards the centre of the trap by the gradient forces. The same cannot be said for the $z$component of the optical torque; while this effect could still be attributed to the spin-curl force, but it is clear that the internal scattering between the two spheres has some unintended effects.

By repeating the same kinds of simulation as used in 4.5 but for a circularly polarised beam $\phi = 90\circ$ it was found that not only is the rotation rate dependent on the size of the dimer, but also on its orientation and therefore their axial position.

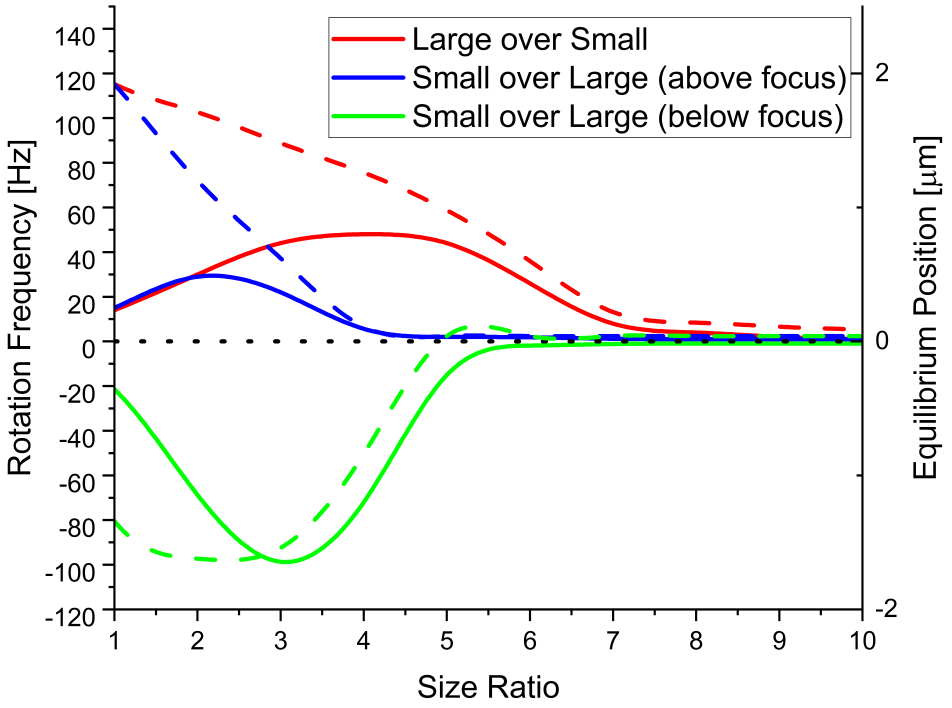

Figure 4.8: Rotation rate plotted against dimer size ratio while trapped in a circularly polarised beam; a positive rotation rate indicates clockwise rotation, whereas a negative rotation rate indicates counter-clockwise rotation. The red line is for the case of a dimer in its 'standard' orientation. The blue line is for the case when the dimer is in its 'inverted' orientation while trapped above the focus of the beam. And lastly the green line is for the case when the dimer is in its 'inverted' orientation, but when it is trapped below the focus of the beam.

It is difficult to see from the graph, but the rotation rate never truly goes down to zero, reaching a minimum of 2 Hz, which would imply that a second sphere of radius 200 nm is enough to induce rotational motion. This brings into question what mechanism is generating the optical torque. We used *mstm* to look at the stokes parameters from the scattered field from a simple plane wave incident on a symmetric dimer, the proportion of circularly polarised light is minimal compared to the proportion of plane polarised light, which indicates that this rotational motion is not due to any inhomogeneity in the dimer that might impart angular momentum to the scattered beam - as compared to a anisotropic scatterer like vaterite. Therefore the rotational motion must be due to

These results are somewhat contradictory to other work with silica dimers [1, 6, 14]; previous experiments have trapped the dimer in an orientation perpendicular to the beam propagation direction. The rotational motion is attributed to the dimers asymmetric geometry creating an unbalanced polarisation susceptibility along its long axis as compared to its short axis; therefore its long axis is aligned with the polarisation vector and can rotate freely [1]. This however cannot be the case with our simulations as the dimer rotates about its long axis, meaning there cannot be an asymmetric axis to align with the beam's polarisation vector. Furthermore, we see a non-linear increase in the rotational speed of our dimers with size, the drag torque from the surrounding fluid is $\propto r^3$ so the expectation is that the rotation frequency should fall off with increasing size. This indicates that the rotational motion is due to the shape asymmetry of the dimer and not solely due to the beam's angular momentum. Measurement of this photokinetic force is difficult to achieve due to the fact that previous analysis was conducted in the Rayleigh regime, where the polarizability of our dimer can be approximated as:

$$\mathbf{p}(\mathbf{r},t) = \alpha_x E_x(\mathbf{r},t)\hat{\mathbf{e}}_x + \alpha_y E_y(\mathbf{r},t)\hat{\mathbf{e}}_y + \alpha_z E_z(\mathbf{r},t)\hat{\mathbf{e}}_z \tag{4.4}$$

where the polarizability is given as a 3D vector for the three principle Cartesian directions. In order to measure the magnitude of second order contributions we would need to construct a dipole array that fully captures the scattering of a dimer. Measuring

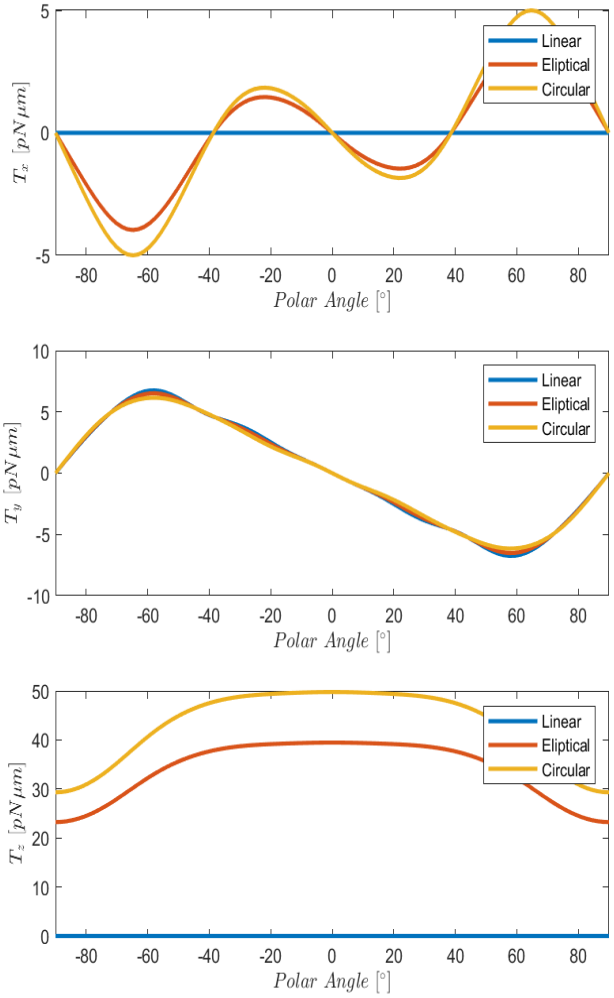

Figure 4.9: Optical torque against polar angle θ about the three primary axis (top: torque about the x-axis; middle: torque about the y-axis; bottom: torque about the z-axis) on a symmetric dimer in linear, elliptical, and circular polarisation beams. Diagram to the right is for visual clarity about the direction of θ.

the optical torque makes it clear that the polarizability is a contributing factor to this optical rotation phenomena. Rotating a symmetric dimer in the $x-z$ plane reveals that while the dimer can be rotated in an orientation perpendicular to the beam rotational torque is maximised when rotated while aligned with the optical axis.

4.2.1 Gyroscopic Precession using asymmetric dimers

As mentioned in section 4.1.1 for specificity sized dimers there is the potential for non-vertical trapping orientations in which the dimer is still stably trapped. When a circularly polarised beam is used the dimer exhibits gyroscopic precession. As shown in fig 4.10 the dimer's trajectory exhibits periodic rotation about its long axis U_z, precession motion as the dimer spins around the central beam axis, and nutation motion as the dimer's orientation rocks backwards and forwards.

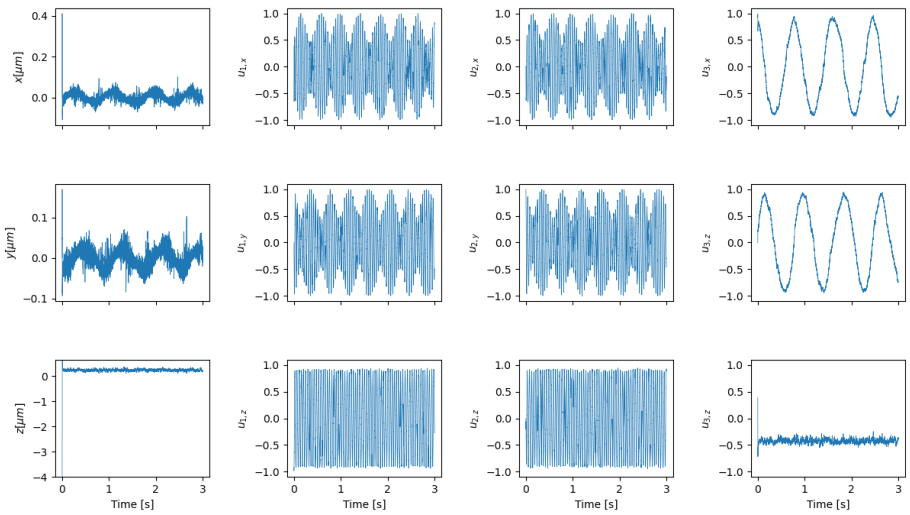

Figure 4.10: 3 second trajectory of a dimer ($a_I/a_{II} = 2$) trapped in an off axis orientation with a circularly polarised beam ($P = 100\ mW$). The far left column depicts the dimer's centre of mass position with time; middle two columns are the x, y, and z components of the vectors u_x and u_y; last column depicts the components of the vector u_z which defines the dimer's orientation.

Applying a Fourier analysis to the above trajectory reveals the 3 fundamental frequencies typically associated with precession; the $u_{z,1}$ and $x(t)$ series show a precession frequency of $1.33\ Hz$ whereas the series $u_{x,1}$ and $u_{y,1}$ show a combined periodic signal - a rotational frequency of $23\ Hz$ and a nutation frequency of $20\ Hz$. Previous studies into amorphous silica nanoparticles found a linear relationship with the rotational frequency and the laser power, but no such relationship existed with the precession frequency. Our own results shows a similar linear relationship with vertically aligned

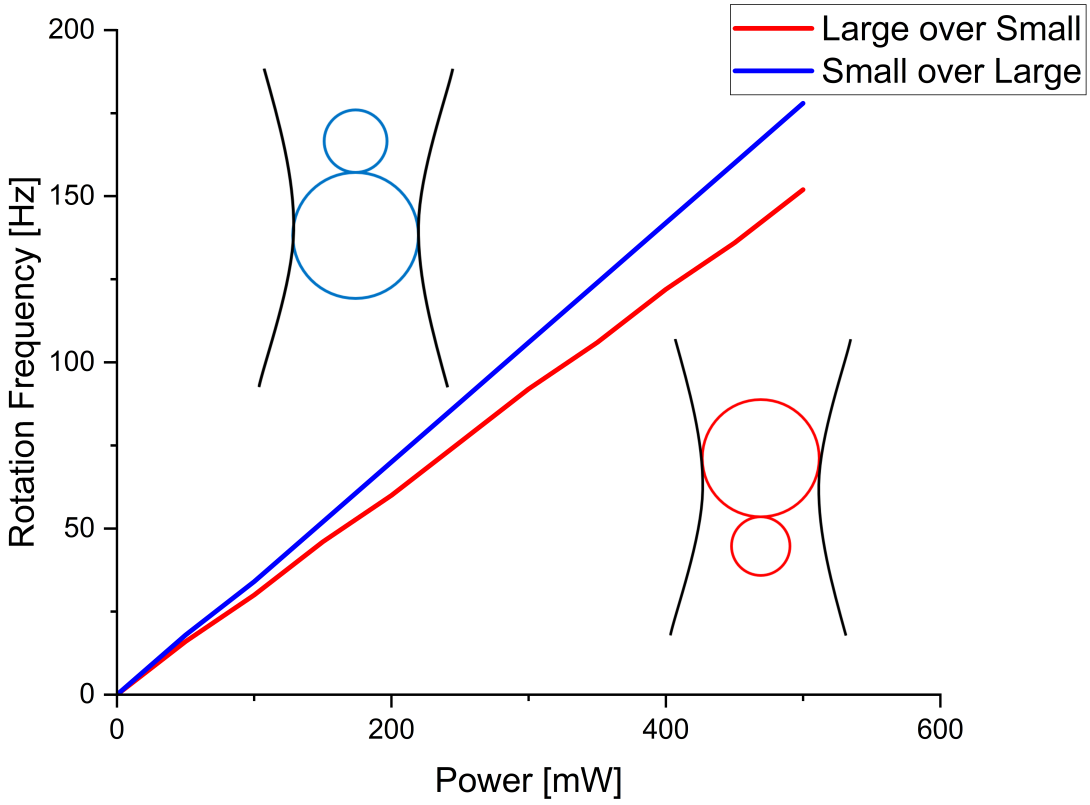

Figure 4.11: Rotational frequency vs laser power for a dimer in both vertical orientations.

dimers.

The linear relationship could partly be due to fact that we do not account for the change in viscous forces with increasing laser power. Due to the localised heating effect It is far more likely that the rotational frequency reaches a maximum value assuming that the bulk fluid can readily absorb the laser.

This gyroscopic motion has been demonstrated previously in nanoparticles [7, 8, 13, 25] but has not been observed for micron scale aggregates. Since the torque applied to the dimer is computed by evaluating the beam coefficients of the scattered field it is difficult to apply this result to micro-rheology experiments as one would need to know the exact magnitude of the optical torque ahead of time in order to make estimations about the local fluid viscosity. This is trivial for a birefringent spherical particle, less so for spherical aggregates whose equilibrium position and orientation are unknown.

However, further analysis of the mechanism behind the precessive motion of off-axis dimers may provide insights into controlling Brownian motion. An experimental work trying to 'cool' nano-dimers by controlling the motion in all 6 degrees of freedom found that even while the rotation about the short axis' could be controlled the free rotation around the dimers' long axis resulted in an unpredictable torsional vibration [2]. Understanding how rotational motion arises in the Mie-Regieme could allow researchers to build a robust theoretical framework to construct beam structures that eliminate any unwanted rotational motion from a target particle. Conversely, the same framework could allow for precise measurements of the optical torque applied to a target particle, allowing for characterisation of complex shaped particles' interactions with an optical trap.

4.3 Characterisation of asymmetric dimers via PSD analysis

As discussed in **??**, one of the methods developed to work in conjunction with [19] is a simulated quadrant photo diode for as a position detection system. While it is possible to extract all of the relevant dynamical information from a simulation, confirming the same behaviour in an experimental setting can be challenging if dealing with a non-birefringent particle.

As a benchmark we start by considering a single sphere within an optical trap. A single polystyrene sphere suspended in water ($a = 1\mu m$, $n_p = 1.59$, $n_m = 1.33$) is trapped by a focus Gaussian beam and its trajectory was recorded. A 3 second is trajectory is a typical measurement time for collecting a power spectrum, the spectra was fitted to eq. **??**.

As shown in fig. 4.12, the two power spectra report different corner frequencies which would be indicate that the trap is not perfectly circular. Using *ott* we can compare the expected trap strength to what is reported by a quadrant photo diode:

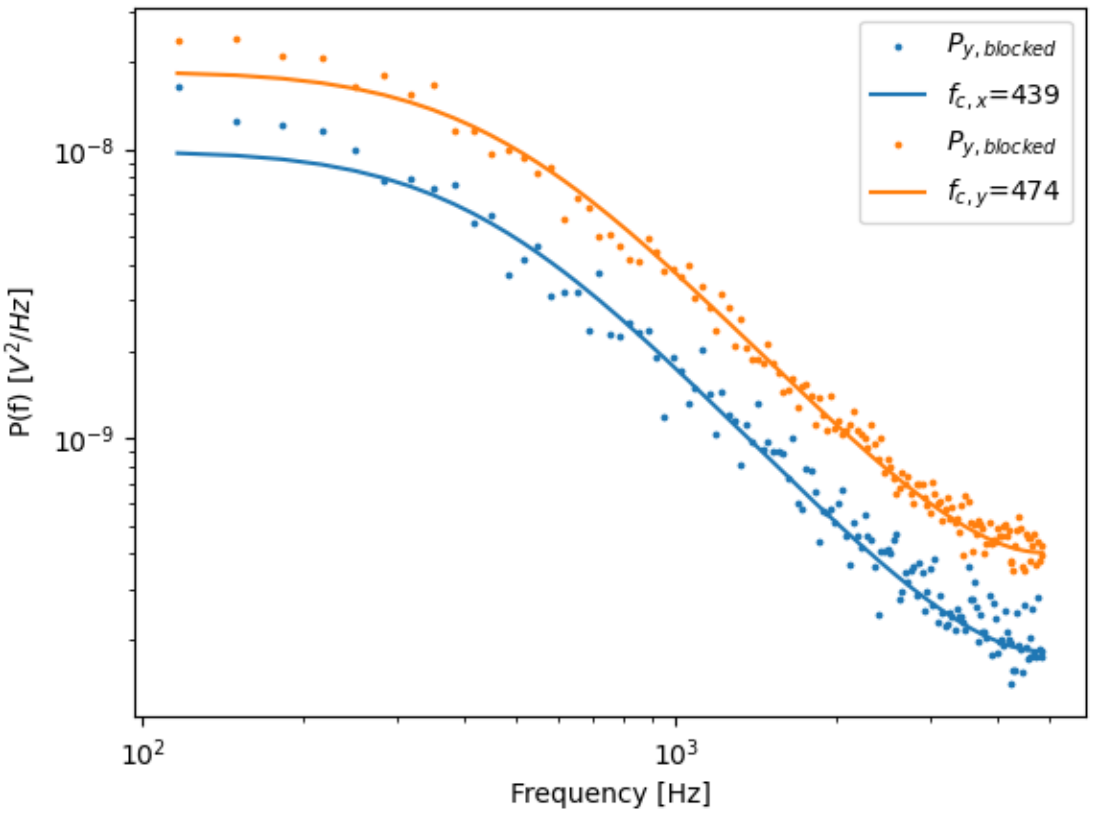

Figure 4.12: Recorded power spectra fitted to eq. **??**, scattered points represents the blocked data ($n_b = 100$). Corner frequency for the Lorentzian curves are reported in the legend.

Fitting parameter	*ott* estimates		QPD fitting		Simulation fitting	
$f_c\ [Hz]$	447	450	439	474	523	513
$\kappa\ [pN/\mu m]$	53.05	53.40	51.96	56.09	61.94	60.7
Ellipticity	8.16 %		27.17 %		13.8 %	

Where the ellipticity of the beam is given by $e = (1 - \kappa_y/\kappa_x)^{0.5}$ and is a measure of the symmetry of the beam wavefront. Its clear from these initial results that the QPD is more sensitive to changes along the y-axis than the x-axis when compared to the direct *ott* calculations. Typically, even an industrial Gaussian beam will produce an elliptical diffraction limit spot when heavily focused; in their tutorial for optimizing the PSD analysis, Berg and Sorensen reported a ellipticity of around 15 % after a total calibration time of 81 seconds [3]. The reason for this discrepancy can be explained

partly by the fact that our estimation of the trap geometry via *ott* is based on the force-displacement curve while the sphere is moving in only one direction, whereas the QPD is estimating the trap geometry by extrapolating from far field scattering signals. We now consider a symmetric dimer in identical simulative conditions.

Fitting parameter	*ott* estimate		QPD fitting		Simulation fitting	
f_c $[Hz]$	409	334	431	424	274	285
κ $[pN/\mu m]$	48.51	39.58	51.13	50.26	32.45	33.75
Ellipticity	42.8 %		12.7 %		13.8 %	

Now we see that the *ott* predicts a more elliptical trap compared to the QPD model which says the trap is far more symmetrical while trapping a symmetric dimer. A potential reason that *ott* no longer expects a circular trap could be due to how it computes the beam shape coefficients; by point matching in the far field before the focus means a loss in accuracy for objects that trap above the focus. The change in the QPD estimation can be partially explained by the fact that rotational effects are not accounted for in the Lorentzian power spectra, only translational motion. Typically, rotational motion is only ever detected when it is periodic (take for example Fig. **??**), when the motion is stochastic the entire power spectra is effected making it near impossible to separate the translational and rotational contributions from a single power spectra.

4.4 Conclusions

Considering the simplicity of a scatterer such as a dimer, one would assume that the dynamics of such an object would be relatively easy to predict. Simulations of dimers in the Mie regime show that not only do they have multiple positions and orientations in which they can be trapped but also that their interaction with circularly polarised light is heavily dependent on the axial position and trapping orientation. Dimer's have the potential to be used as adaptive micro-rotors, being simple to synthesise and can be made out of any material of choice, but in order for these particles to be used as such one needs a means of characterising the optical torque applied. While estimations can be made in the Rayleigh regime due to the dimer being treated as point dipole,

Mie regime micro rotors require an in-depth theoretical description of the mechanism that is creating this optical torque.

Bibliography

[1] J. Ahn, Z. Xu, J. Bang, Y.-H. Deng, T. M. Hoang, Q. Han, R.-M. Ma, and T. Li. Optically levitated nanodumbbell torsion balance and ghz nanomechanical rotor. *Physical Review Letters*, 121(3):033603, July 2018.

[2] J. Bang, T. Seberson, P. Ju, J. Ahn, Z. Xu, X. Gao, F. Robicheaux, and T. Li. Five-dimensional cooling and nonlinear dynamics of an optically levitated nanodumbbell. *Physical Review Research*, 2(4):043054, Oct. 2020.

[3] K. Berg-Sørensen and H. Flyvbjerg. Power spectrum analysis for optical tweezers. 75:594–612, 2004.

[4] A. A. Bui, A. B. Stilgoe, I. C. Lenton, L. J. Gibson, A. V. Kashchuk, S. Zhang, H. Rubinsztein-Dunlop, and T. A. Nieminen. Theory and practice of simulation of optical tweezers. *Journal of Quantitative Spectroscopy and Radiative Transfer*, 195:66–75, July 2017.

[5] C. D, P. P, N. B V, S. Bhattacharya, and S. Ananthamurthy. Laser polarization driven micromanipulation and reorientation dynamics of an asymmetric shaped microscopic biomaterial using optical tweezers. *Journal of Optics*, 24(9):094007, Aug. 2022.

[6] R. Debuysschère, B. Rimez, A. Zaccone, and B. Scheid. Experimental and theoretical investigation of nonclassical shear-induced nucleation mechanism for small molecule. *Crystal Growth & Design*, 23(7):4979–4989, June 2023.

[7] T. M. Hoang, Y. Ma, J. Ahn, J. Bang, F. Robicheaux, Z.-Q. Yin, and T. Li. Torsional optomechanics of a levitated nonspherical nanoparticle. *Physical Review Letters*, 117(12):123604, Sept. 2016.

[8] S. Kuhn, A. Kosloff, B. A. Stickler, F. Patolsky, K. Hornberger, M. Arndt, and J. Millen. Full rotational control of levitated silicon nanorods. 2016.

[9] M. Li and J. Arlt. Trapping multiple particles in single optical tweezers. 281:135–140, 2008.

[10] J. C. Loudet, B. M. Mihiretie, and B. Pouligny. Optically driven oscillations of ellipsoidal particles. part ii: Ray-optics calculations. 37, 2014.

[11] P. Praveen, Yogesha, S. S. Iyengar, S. Bhattacharya, and S. Ananthamurthy. Two particle tracking and detection in a single gaussian beam optical trap. 55:585, 2016.

[12] A. A. Ranha Neves and C. L. Cesar. Analytical calculation of optical forces on spherical particles in optical tweezers: tutorial. *Journal of the Optical Society of America B*, 36(6):1525, May 2019.

[13] M. Rashid, M. Toroš, A. Setter, and H. Ulbricht. Precession motion in levitated optomechanics. *Physical Review Letters*, 121(25):253601, Dec. 2018.

[14] R. Reimann, M. Doderer, E. Hebestreit, R. Diehl, M. Frimmer, D. Windey, F. Tebbenjohanns, and L. Novotny. Ghz rotation of an optically trapped nanoparticle in vacuum. *Physical Review Letters*, 121(3):033602, July 2018.

[15] D. B. Ruffner and D. G. Grier. Optical forces and torques in nonuniform beams of light. *Physical Review Letters*, 108(17):173602, Apr. 2012.

[16] V. Shahabadi and E. Madadi. Effective multiple optical trapping of sub-micrometer particles with petal beams. *Journal of the Optical Society of America B*, 37(12):3665, Nov. 2020.

[17] X. Sheng-Hua, L. Yin-Mei, L. Li-Ren, and S. Zhi-Wei. Computer simulation of the collision frequency of two particles in optical tweezers. 14:382–385, 2005.

[18] B. Silverman. *Denisty Estimation for Statistical and Data Analysis*. Chapman and Hall, 1986.

[19] W. Vigilante, O. Lopez, and J. Fung. Brownian dynamics simulations of sphere clusters in optical tweezers. *Optics Express*, 28(24):36131, Nov 2020.

[20] X.-L. Wang, J. Chen, Y. Li, J. Ding, C.-S. Guo, and H.-T. Wang. Optical orbital angular momentum from the curl of polarization. *Physical Review Letters*, 105(25):253602, Dec. 2010.

[21] S. Xu, Y. Li, and L. Lou. Axial optical trapping forces on two particles trapped simultaneously by optical tweezers. 44:2667, 2005.

[22] A. Yevick, D. J. Evans, and D. G. Grier. Photokinetic analysis of the forces and torques exerted by optical tweezers carrying angular momentum. *Philosophical Transactions of the Royal Society A: Mathematical, Physical and Engineering Sciences*, 375(2087):20150432, Feb. 2017.

[23] Y. Zhao, J. S. Edgar, G. D. M. Jeffries, D. McGloin, and D. T. Chiu. Spin-to-orbital angular momentum conversion in a strongly focused optical beam. *Physical Review Letters*, 99(7):073901, Aug. 2007.

[24] Y. Zhao, D. Shapiro, D. Mcgloin, D. T. Chiu, and S. Marchesini. Direct observation of the transfer of orbital angular momentum to metal particles from a focused circularly polarized gaussian beam. *Optics Express*, 17(25):23316, Dec. 2009.

[25] Q. Zhu, N. Li, H. Su, W. Li, and H. Hu. Dynamic analysis and simulation of an optically levitated rotating ellipsoid rotor in liquid medium. *Photonic Sensors*, 12(2):105–116, Sept. 2021.